Landslide Monitoring Using Hybrid Conventional and Persistent Scatterer Interferometry

Maryam Dehghani[1]

Abstract The Kahroud region located in the Alborz Mountains, northern Iran is subject to landslide. In this paper, the impact of two different Persistent Scatterer Interferometry methods on the study area is examined. The standard Stanford method for Persistent Scatterer (StaMPS) was applied to 14 ENVISAT ASAR images spanning between 2006 and 2008, but it was found that the displacement was underestimated due to a high deformation rate. A hybrid method that is a combination of conventional and PSI methods was then applied to the study area. In this method, the deformation rate roughly estimated by stacking the coherent interferograms characterized by small baselines was estimated and subtracted from the wrapped phase. The residual phase was then unwrapped using the standard StaMPS. The estimated rate was finally added back to the unwrapped residual phase. The maximum Line-Of-Sight (LOS) deformation rate estimated from the hybrid method was 25 mm/year, belonging to an area located in the lower part of the landslide. The deformation time series of a couple of distinct points showed differing behavior in different time periods. However, the area was still found to be generally sliding toward the satellite. These results were validated with GPS measurements at 7 stations. The Root Mean Square Error (RMSE) between LOS GPS-derived rates and rates estimated from the hybrid method was estimated as 4 mm/year.

✉ Maryam Dehghani
Dehghani_rsgsi@yahoo.com

[1] Department of Civil and Environmental Engineering, School of Engineering, Shiraz University, Engineering Building 1, Namazi Sq., Zand Ave., Shiraz, Iran

Introduction

The term "landslide" describes a wide variety of processes that result in the downward and outward movement of slope-forming materials including rock, soil, artificial fill, or a combination of these. The materials may move by falling, toppling, sliding, spreading, or flowing (Indirli et al. 2010). Although many types of slope movement are not actually considered landslides, a rather general description of a landslide can be expressed as a geotechnical phenomenon which occurs when a natural or artificial slope loses its stability under a number of different factors, such as excessive shear stresses, gravitational forces, excess pore water pressure development, seismic loads, and a number of other factors, which overcome the resistance of the soil along a so-called failure surface, or the slip plane. In this regard, Cruden (1991) provides a simple description of this phenomenon as the flow of a mass of rock, debris or earth down a slope (Cruden 1991; Cornforth 2005).

The mountainous areas of Iran are highly subject to landslide. One of these areas, i.e. Kahroud, is located in the Alborz Mountains found in northern Iran. The geology map (scale, 1:100,000) of the Kahroud area is shown in Fig. 1. The village of Kahroud is located in the valley exactly below the landslide area. The landslide area is surrounded by sedimentary rock type including shale, sandstone, siltstone, carbonaceous shale, claystone, quartzite and conglomerate. The south of the area is covered by lava, mainly trachyandesitic and trachytic flows. The Barzadeh anticline is passed through the area subject to rock fall, while the Panjab anticline is located to the north of the study area.
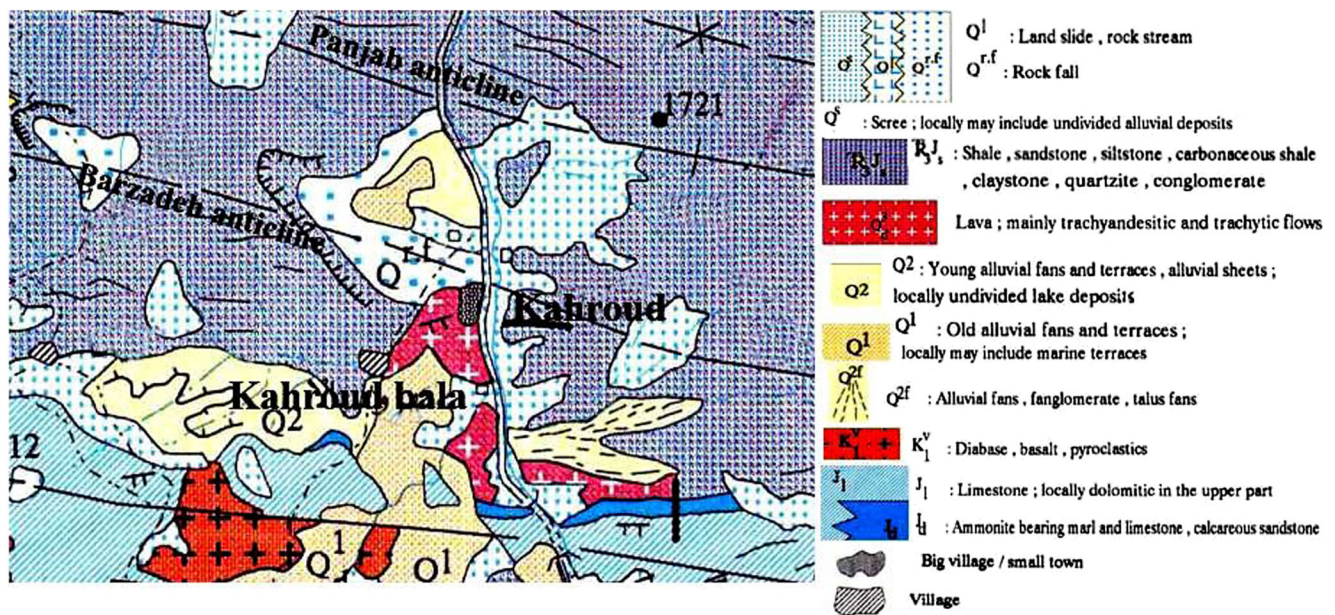
Fig. 1 Geology map of the study area (scale: 1:100,000)

Billions of dollars are lost each year due to landslide damage (Fig. 2). Thus, the monitoring of landslides is essential if warning systems are to work efficiently. In 2003, 8 GPS stations were installed on the site of Kahroud to measure the deformation caused by landslide. A field photograph of the landslide is presented in Fig. 3 (Peyret et al. 2008).

The GPS measurements were carried out over a 1-year period (Peyret et al. 2008). Moreover, the network was densified (57 marks) and measured twice in 6 months using a rapid static approach. It should be noted, however, that GPS measurements and precise leveling observations measure the deformation at only a few sparse locations, i.e. stations and benchmarks. Moreover, surveys to collect the observation data can prove exceedingly costly and time-consuming.

Among various ground- and spaced-based techniques available, the Interferometric Synthetic Aperture Radar (InSAR) technique has demonstrated its ability to measure deformation over large areas and at high spatial resolution (Peltzer et al. 1998; Fruneau and Sarti 2000; Tesauro et al. 2000; Crosetto et al. 2002; Chatterjee et al. 2006). Various studies have used the InSAR technique to both detect and monitor landslide. To illustrate, a landslide in the Swiss Alps was studied using the InSAR technique. Input maps were generated by means of ERS for landslide susceptibility assessment purposes. A land cover map was then generated via image classification of multi-temporal intensity images in combination with coherence images. Other input maps such as those pertaining to slope, aspect and relief were extracted from InSAR DEM. Finally, the susceptibility maps were generated using the input maps (Singh 2003).

Fig. 2 An example of damage caused by landslide (Brazil)

Fig. 3 A field photograph of the Kahroud landslide. The red line shows the landslide boundary (Peyret et al. 2008)

As regards the present study, the spatial and temporal behavior of the Kahroud landslide was monitored using the InSAR technique (Peyret et al. 2008). Conventional InSAR techniques were applied using Envisat ASAR images. 35-day interferograms were utilized in stacking to measure the landslide rate. However, the deformation time series could not be obtained using InSAR. As such, GPS measurements spanning the aforementioned period were also applied to monitor the Kahroud Landslide.

Conventional interferometry fails to measure deformation in the case of loss of correlation (Galloway and Hoffmann 2007). One of the sources of decorrelation is look angle error, an issue which typically occurs in mountainous areas. Persistent Scatterer InSAR (PSI) is a recently developed technique used to address the problem of decorrelation by identifying scatterers, called Persistent Scatterers (PSs), the echo of which varies little in time (Ferretti et al. 2000; Hooper et al. 2004; Kampes 2005).

Several studies have been carried out using PS interferometry. Slow slope movements in Alpine areas were measured based on interferograms derived from ERS repeat pass SAR data. The PS technique, benefitting from long time series of SAR images, was applied to map ground deformation at millimetric accuracy. Several slides in the Pennine Alps, Switzerland were detected using interferograms of annual time span. The highest velocity of 4 cm/year was found in this area (Rott et al. 2003). PS interferometry was also applied to the Penitencia Creek landslide located in the hills east of San Jose, CA. Deformation rates of about 0.5 cm/year were estimated. In another study carried out by Ferretti et al. in 2000 and 2001, 48 ERS-1/2 SAR images spanning from 1992 to 2001 were analyzed to evaluate landslide movements over an area of 54 km^2. The majority of PS points in the study area displayed LOS deformation rates close to zero. Most of the PSs within the landslide area contain LOS deformation rates on the order of 0.15 to 0.25 cm/year. Moreover, PS analysis indicated a zone of large deformation in the north part of the mapped limits of the landslide, with deformation rates on the order of 0.25 to 0.4 cm/year.

Several PSI approaches have been proposed so as to identify PS pixels and estimate the deformation signal (Ferretti et al. 2001; Hooper et al. 2007; Ketelaar 2009). These methods differ primarily in the PS selection algorithm and deformation estimation. In some PS algorithms, a temporal model for deformation is utilized to identify the PS pixels and estimate the unknown parameters, including phase ambiguities. In these methods, only scatterers with a deformation behavior close to the assumed model are identified as PS. Moreover, PS pixels are detected based on their amplitude information. In this case, only bright scatterers such as man-made features are detected as PS.

A newly-developed algorithm in this regard is the Stanford Method for Persistent Scatterer (StaMPS), capable of benefitting from the spatial correlation between pixels and identifying PSs even in areas such as mountains lacking in man-made features. In StaMPS, no predefined deformation model is required in the PS selection step. However, StaMPS does tend to underestimate displacements when the deformation rate is too high relative to the sampling of the data in time (Dehghani et al. 2013). Therefore, a hybrid method consisting of both conventional and StaMPS techniques was proposed by Dehghani et al. (2013) in the event that high rates of deformation were encountered. According to the study already carried out on the Kahroud landslide using radar images belonging to 2006, the landslide rate was estimated as several centimeters. Since this rate is relatively high, presumably standard StaMPS cannot be expected to function 100 % accurately in the area. Therefore, in this paper, both standard and hybrid algorithms were used in order to detect and measure the deformation of Kahroud landslide. Both methods were employed using radar images spanning between September 24, 2006 and July 20, 2008 and the results were compared. The landslide rate denoting long-term deformation behavior was extracted. Moreover, the short-term deformation behavior of a couple of PS pixels was studied via time series analysis.

SAR Interferometry Method

A deformation map is obtained by differencing the phase measurements from two radar images acquired at different times. The phase difference, known as interferometric phase, contains different constituents as follows:

$$\psi_{x,i} = W\{\phi_{D,x,i} + \phi_{A,x,i} + \Delta\phi_{S,x,i} + \Delta\phi_{\theta,x,i} + \phi_{N,x,i}\} \quad (1)$$

Where $\phi_{D,x,i}$ is the phase of ground surface deformation, $\phi_{A,x,i}$ is the phase resulting from the atmosphere caused by the different atmospheric delay, $\Delta\phi_{S,x,i}$ is the orbital error, $\Delta\phi_{\theta,x,i}$ is the phase resulting from the look angle error caused by the residual topography, and $\phi_{N,x,i}$ is the noise caused by decorrelation. $W\{.\}$ is the wrapping operator. Phase unwrapping solves the number of phase cycles detected by the radar.

Conventional interferometry can only be used in areas not suffering from decorrelation, the causes of which are look angle errors and vegetation coverage in mountainous areas. Decorrelation causes conventional interferometry to fail to operate properly.

In the late 1990s, it was found that there are targets whose backscattering behaviour varies little over time. These targets
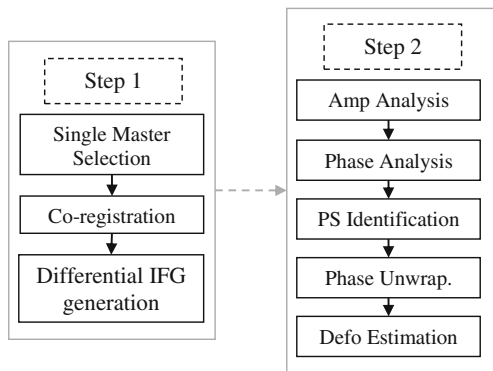
Fig. 4 Block diagram of the standard StaMPS. IFG: interferogram, Amp: amplitude, Defo: deformation

are called Persistent Scatterers (PS). Several Persistent Scatterer Interferometry (PSI) methods have been developed since then. A newly developed method called StaMPS and introduced by Hooper et al. (2004) can be successfully applied to areas lacking in bright features. Furthermore, no deformation model is applied in the PS identification step and unknown parameter estimation. Therefore, PS pixels with different deformation behavior can be selected. There are two main steps in the StaMPS as follows (Fig. 4).

Interferogram generation

The interferograms are generated using an image as a single master. The master image is selected to maximize stack coherence, which is a function of temporal and perpendicular baselines and Doppler centroid frequency (e.g., Kampes 2005; Ketelaar 2009). The images are co-registered to the master using a novel method developed by Hooper et al. 2004. In this method, the offsets between pairs of images with high correlations are estimated. The function mapping the master image to each of the other images is then estimated by means of least square inversion. In order to generate the differential interferograms, the Shuttle Radar Topography Mission (SRTM) DEM is used to remove the main topographic contribution to the interferometric phase.
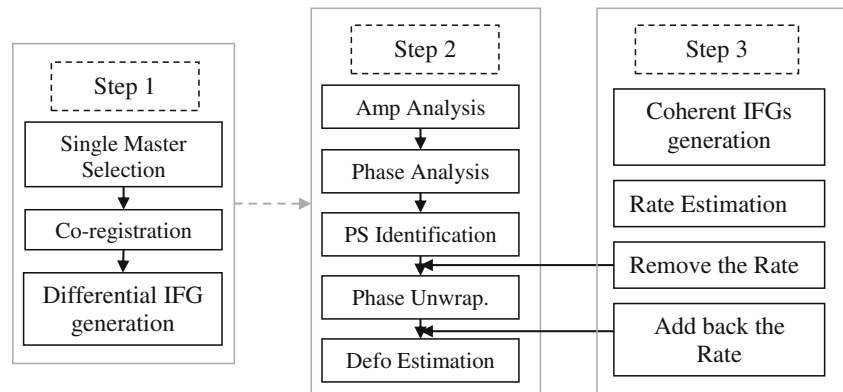
PS identification and deformation estimation

In this step, the StaMPS is applied to select PS pixels and deformation estimation. The initial PS candidates are selected according to their amplitude information using the amplitude dispersion index with a threshold of 0.4 (Ferretti et al. 2001). The final PS pixels are identified based on phase stability analysis assuming that the acceptable fraction of false positive identification, i.e. the fraction of pixels selected as PS that are actually non-PS pixels, is 1 %. In phase stability analysis, $\phi_{N,x,i}$ in Eq. (1) determines whether a candidate is a PS or not. The phase noise component for each candidate is estimated by subtracting as much of the spatially-correlated phase components as possible in an iterative manner.

In each iteration, a measure of the variation of the phase noise is calculated. PS pixels are finally selected according to the probability of being PS estimated from the amplitude dispersion and phase noise variation. The spatially-uncorrelated part of the look angle error, $\Delta\phi^u_{\theta,x,i}$, and the master contribution to the spatially-correlated part of the signal, $\phi^{m,u}_x$, are then estimated and subtracted from the interferometric phase.

The phase unwrapping process involves two steps. In the first step, the phase difference between nearby pixels is unwrapped over time based on the Nyquist sampling criterion. For the phase unwrapping algorithm to have any chance of success, the evolution of the phase difference between it and at least one neighboring PS pixel must be less than half a cycle between acquisitions for each PS pixel (Nyquist sampling theorem). For the C-band data used in this study, half a cycle is equivalent to displacement of 1.4 cm. When the deformation exceeds this limit, the Nyquist sampling criterion is not met. In the second step, a probability density function is constructed using the unwrapped time series of differenced phases. These are converted into cost functions and fed into the optimization routines of the 2-D statistical-cost network-flow algorithm presented by Chen and Zebker (2001) (Hooper 2010).

In order to estimate the phase contribution caused by deformation, spatially correlated nuisance terms are finally
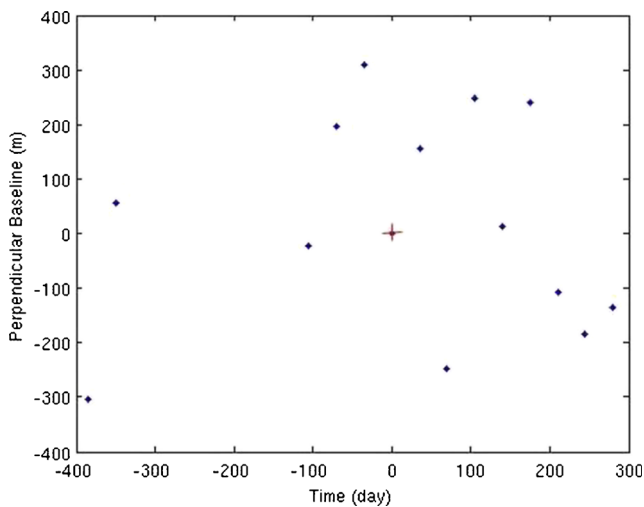
Fig. 5 Block diagram of the hybrid method. IFG: interferogram, Amp: amplitude, Defo: deformation

Fig. 6 Acquisition geometry of available data in the area: temporal baselines against perpendicular baselines. The cross sign (+) represents the master image

Table 1 Coherent small baseline interferograms list. Each master and slave acquisition belongs to an interferogram

Master	Slave
20060924	20061029
20061029	20070701
20070701	20070805
20070701	20071014
20070805	20070909
20070805	20071118
20070909	20071118
20070909	20080127
20071014	20071118
20071014	20080302
20071118	20080127
20071118	20080406
20071223	20080615
20080127	20080406
20080302	20080511
20080511	20080720
20080615	20080720
20080511	20080615

estimated by means of spatial and temporal filtering and subtracted from the unwrapped phase. In the last step, the estimated phase values are converted into the displacement signal via a multiplication by the conversion factor $\frac{4\pi}{\lambda}$.

The individual coherent interferograms characterized by small baselines can be unwrapped spatially. If the deformation is too high, the standard StaMPS underestimates the displacement rate because the Nyquist sampling criterion cannot be met in the unwrapping step. Therefore, a hybrid method has been presented by Dehghani et al. (2013) to overcome the Nyquist problem. In the hybrid method, the deformation rate present in the data is first reduced. This rate, which is the linear component of the deformation, is estimated from the individually unwrapped coherent interferograms using stacking. The estimated rate is then subtracted modulo-2π from each wrapped interferogram. It should be noted that the main part of the wrapped deformation signal is removed from the original wrapped phase. The standard StaMPS is then applied to the residual phase. Finally, the linear term is added back to the
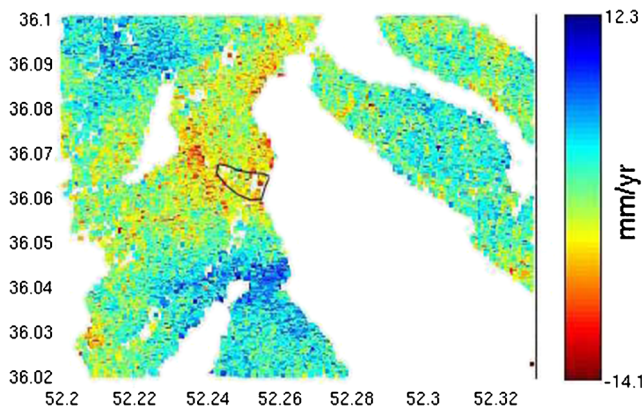
unwrapped residual phase. The steps of this hybrid method are shown in Fig. 5.

In the present study, both the standard StaMPS and hybrid methods were applied to the available dataset and the results were compared.

Results and Discussion

The standard StaMPS and hybrid methods were implemented on the interferometric data of the Kahroud area. 14 Envisat ASAR images of Track 285 acquired between September 24, 2006 and July 20, 2008 were used to generate 13 differential interferograms. Figure 6 depicts the acquisition geometry of the available dataset. The
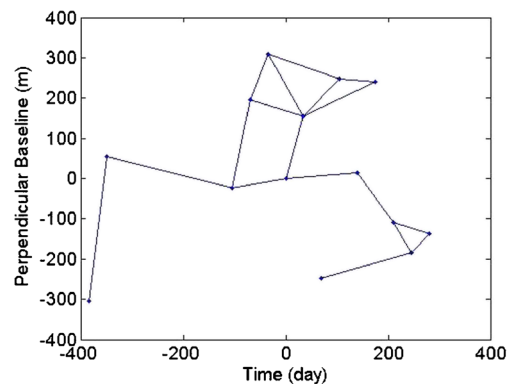

Fig. 7 Mean displacement velocity map obtained from the standard StaMPS. The black polygon shows the outline of Kahroud landslide

Fig. 8 Time vs spatial baselines for coherent interferograms. The connections represent the coherent processed interferograms

Fig. 9 Mean displacement velocity map obtained from the hybrid method. The black polygon shows the outline of Kahroud landslide
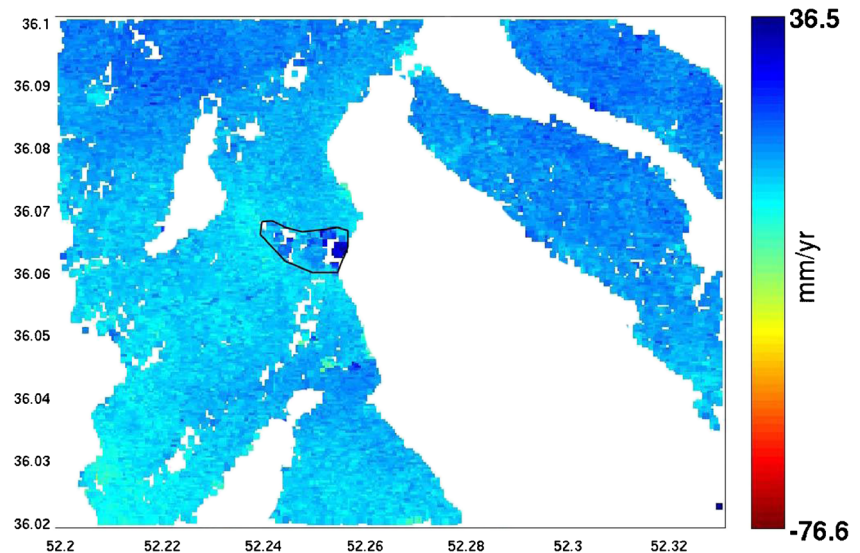
acquisition mode of the dataset was ascending (incidence angle: 23°). The master image selected to maximize stack coherence dates back to October 14, 2007.

Amplitude analysis based on amplitude dispersion with a threshold of 0.4 was applied to select the PS candidates. The final group of PS pixels was identified according to phase stability analysis. As a result, 64368 pixels were detected to be of the PS variety. The PS density varied from low to high across the study area. The mean displacement velocity map obtained from the standard StaMPS is illustrated in Fig. 7. The black polygon shows the limit of the landslide. Accordingly, no significant deformation could be detected. The estimated deformation rate was very low compared to some of the individual interferograms generated by the conventional InSAR.

If the process of temporal data sampling is not suitable enough to capture the detailed variation of the deformation, nonlinear deformation fluctuations may leak into the estimates of other temporally uncorrelated signals such as the atmospheric signal of the slave images. This phenomenon may lead to the observation of the deformation signal in the estimated atmospheric signal of the slave images (for more information, refer to Hooper et al. 2007 and Dehghani et al. 2013). Therefore, the slave contribution to the atmospheric term was not estimated and removed from the velocity, meaning that some signals can be observed beyond the limit of the landslide area, which in fact is due to the atmospheric effect. It should be noted that these signals do not have fixed locations in all interferograms.

Because the estimated deformation rate is very low, it is likely masked by the atmospheric signal.

Alongside the standard StaMPS, the hybrid method was also applied on the dataset since it was assumed that the deformation rate is very high such that the Nyquist criterion cannot be met. In this method, 18 coherent small baseline interferograms were generated and individually unwrapped

(Table 1). The time versus spatial baselines for the coherent interferograms are shown in Fig. 8.

The deformation rate was estimated using an interferogram stacking approach as follows:

$$\widehat{\dot{\phi}}_x = \frac{\sum_{k=1}^{N} \phi_x{}^k}{\sum_{k=1}^{N} t^k} \qquad (2)$$

where $\phi_x{}^k$ is the observed phase of the kth coherent differential interferogram calculated over a time period of t^k, N is the number of coherent interferograms, and $\widehat{\dot{\phi}}_x$ is the estimated deformation rate. The deformation rate was then subtracted modulo-2π from each wrapped phase of PS pixel. After
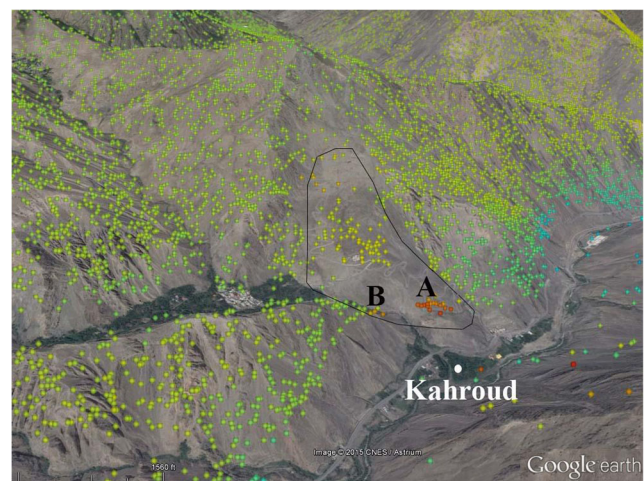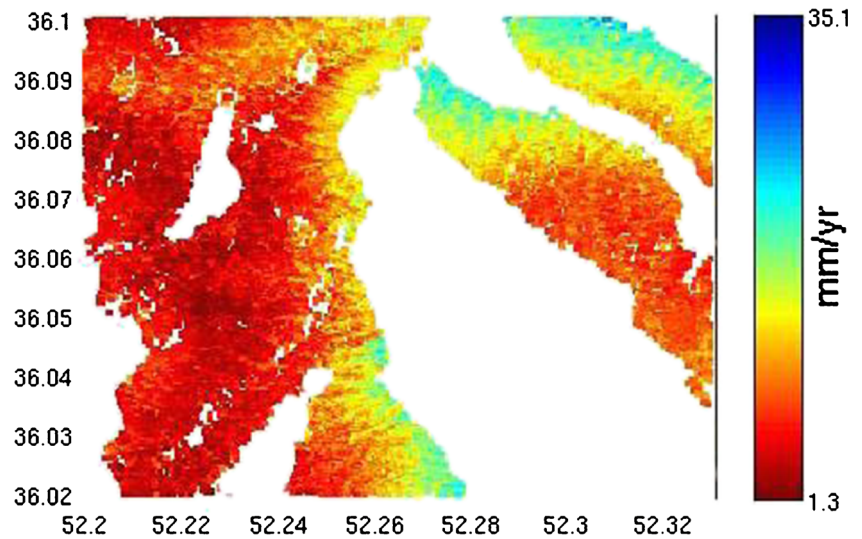

Fig. 10 PS points superimposed on a 3D high-resolution satellite image. The orange points within the polygon above Kahroud village show the landslide area

Fig. 11 standard deviation of the mean LOS velocity calculated using the percentile bootstrap method

unwrapping the residual phase, the deformation rate was added back. The results obtained from the hybrid method are illustrated in Fig. 9. As observed, the deformation due to the Kahroud landslide can be detected in the velocity map. The maximum deformation rate was estimated as ~25 mm/year. The PS points are superimposed on 3D high-resolution satellite imagery in order to indicate the exact landslide location (Fig. 10). The yellow and orange points within the polygon above Kahroud village depict the landslide location.

A comparison of Figs. 7 and 9 reveals that the deformation rates estimated from both methods are completely different. The deformation rate estimated using the hybrid method is much higher than that obtained from the standard StaMPS approach. Some of the coherent individual interferograms, i.e. 20071014_20071118 and 20080615_20080720, prove that the deformation is indeed significant. For example, the displacement of the earth's surface was 5 cm within 35 days, indicating that the standard StaMPS is clearly underestimating the deformation rate due to the Nyquist criterion problem.

The standard deviation of the mean LOS velocity estimated for every pixel using the percentile bootstrap method is illustrated in Fig. 11 (Efron and Tibshirani 1986). The standard deviation in most parts of the area is less than 1.5 mm/year except for a small number of pixels which are likely not of the PS variety. Fortunately, the Kahroud landslide area is located on a slope not subject to foreshortening. The areas lying on the slopes oriented towards the west are foreshortened. Only a small number of pixels in these slopes were identified as PS. These pixels have subsequently been removed from the results.

The mean velocity map allows for the identification of long-term average deformation. However, the main strength of time series analysis is its potential to detect deformation signals that are not steady in time (e.g. Lanari et al. 2004). To study the evolution of deformation, time-series plots of a selection of points located within the landslide area were generated. The deformation time series of two points, A and B, whose locations are depicted in Fig. 10, can be seen in Fig. 12. As observed, the points were sliding towards the satellite during the time period of the image acquisition. The deformation behavior of both points is roughly similar. In the generation of the time series plots, the acquisition date of October 14, 2007 was considered as the reference point at which time the deformation is assumed to have been zero. Before this date, the

Fig. 12 Landslide time series of points (a) A and (b) B whose locations are illustrated in Fig. 10
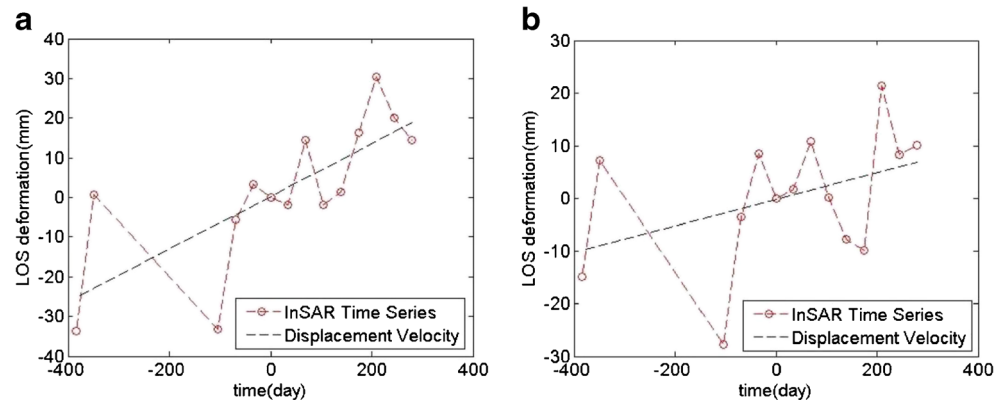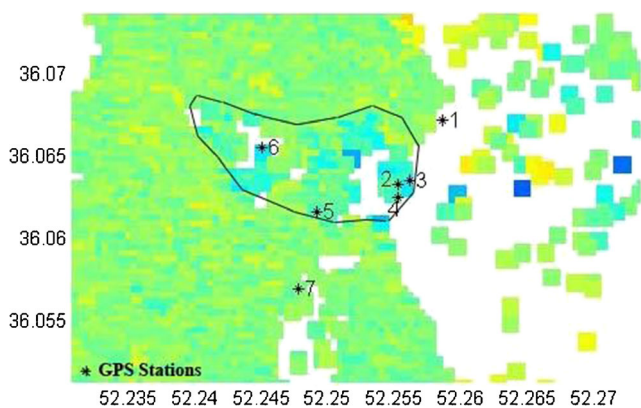
Fig. 13 GPS stations within the study area

Fig. 14 Comparison of landslide rates inferred from the hybrid method and GPS

deformation is negative and after that it is positive. In some specific periods, the deformation rate increases sharply. Moreover, the deformation time series of each point show different behavior in different periods. These fluctuations are observable in the individual interferograms as well. It should be noted that all nuisance terms, including residual topography, master contribution to the atmospheric phase and satellite orbit inaccuracies, were removed from the unwrapped phase. However, deformation fluctuations may still leak into the estimates of other temporally uncorrelated signals such as the atmospheric signal of the slave images. Therefore, the slave atmospheric signal was not removed from the results and was instead treated as correlated noise. As a result, some degree of the time series fluctuations may be due to the atmospheric signal of the slave images.

To validate the results, GPS measurements collected by Peyret et al. (2008) were used. The GPS-derived deformation rates at several GPS stations established within the study area were projected along the radar Line-Of-Sight direction and compared to the hybrid results. The GPS stations are depicted in Fig. 13.

Table 2 compares the LOS GPS-derived deformation rate and hybrid deformation rate at the GPS stations.

Figure 14 presents the deformation rate derived from GPS and the hybrid method. As observed from Fig. 14, all the deformation rates are comparable except in the case of station 6. The spatial pattern of the landslide for the GPS stations broadly agrees with that of the mean velocity map obtained from the hybrid method. The Root Mean Square Error

(RMSE) between the two datasets, excluding station 6, is 4 mm/year.

It should be born in mind that GPS sites provide deformation information at local positions; however, the InSAR measurement at each PS corresponds to a pixel area of $20*20$ m^2. We suspect that this is the primary cause of the rates extracted from two methods not being exactly the same. There are locations within the landslide area with much higher deformation rates in which no GPS stations have been established. These points are observable in the individual interferograms as well as the map of the deformation rate. Therefore, validation of the higher rates was not possible in this study.

Conclusions

In order to study the Kahroud landslide, SAR interferometry was used. Two different methods were applied to the area using 14 ENVISAT ASAR images. The Standard StaMPS tended to underestimate the deformation as compared to the individual interferograms. The hybrid method, which is a combination of conventional and PSI approaches, was then used for time series analysis. The maximum LOS deformation rate belonging to the area in the lower part of the landslide was estimated as 25 mm/year. The time series analysis of several points indicates that the ground surface is generally sliding toward the satellite.

We validated the results of our hybrid method at 7 locations using GPS measurements. The GPS measurements were collected by Peyret et al. (2008). The Root Mean Square Error (RMSE) between the LOS GPS-derived rate and hybrid rate was 4 mm/year. Moreover, the GPS deformation pattern at the stations is broadly in agreement with that obtained from hybrid method.

Nevertheless, monitoring Kahroud landslide using more recent datasets and higher resolution, such as that offered by TerraSAR-x, is essential. TerraSAR-x has a higher revisit

Table 2 LOS GPS derived deformation rate vs. hybrid deformation rate at 7 GPS stations

	#1	#2	#3	#4	#5	#6	#7
GPS LOS rate (mm/year)	−6.011	−2.144	4.1030	3.872	−1.224	−6.123	−0.9310
Hybrid LOS rate (mm/year)	−3.077	4.916	8.152	6.623	5.183	11.992	−0.397

cycle which can result in the Nyquist sampling criterion being met and should be considered for future studies.

References

Chatterjee, R. S., Fruneau, B., Rudnat, J. P., Rpy, P. S., Frison, P. L., Lakhera, R. C., Dadhwal, V. K., & Saha, R. (2006). Subsidence of Kolkata (Calcutta) City, India during the 1990s as observed from space by Differential Synthetic Aperture Radar Interferometry (D-InSAR) technique. *Remote Sensing of Environment, 102*, 176–185.

Chen, C. W., & Zebker, H. A. (2001). Two-dimensional phase unwrapping with use of statistical models for cost functions in nonlinear optimization. *Journal of the Optical Society of America A, 18*(2), 338–351.

Cornforth, D. H. (2005). *Landslides in practice: investigation, analysis and remedial/preventative options in soils*. New York: Wiley.

Crosetto, M., Tscherning, C. C., Crippa, B., & Castillo, M. (2002). Subsidence monitoring using SAR interferometry: reduction of the atmospheric effects using stochastic filtering. *Geophysical Research Letters, 29*(9), 26.1–26.4.

Cruden, D. M. (1991). A simple definition of a landslide. *Bulletin of Engineering Geology and the Environment, 43*(1), 27–29.

Dehghani, M., Valadan Zoej, M. J., Hooper, A., Hanssen, R. F., Entezam, I., & Saatchi, S. (2013). Hybrid conventional and Persistent Scatterer SAR interferometry for land subsidence monitoring in the Tehran Basin, Iran. *ISPRS Journal of Photogrammetry and Remote Sensing, 79*, 157–170.

Efron, B., & Tibshirani, R. (1986). Bootstrap methods for standard errors, confidence intervals, and other measures of statistical accuracy. *Statistical Science, 1*(1), 54–75.

Ferretti, A., Prati, C., & Rocca, F. (2000). Nonlinear subsidence rate estimation using Permanent Scatterers in Differential SAR Interferometry. *IEEE Transactions on Geoscience and Remote Sensing, 38*(5), 2202–2212.

Ferretti, A., Prati, C., & Rocca, F. (2001). Permanent scatterers in SAR interferometry. *IEEE Transactions on Geoscience and Remote Sensing, 39*(1), 8–20.

Fruneau, B., & Sarti, F. (2000). Detection of ground subsidence in the city of Paris using radar interferometry: isolation from atmospheric artifacts using correlation. *Geophysical Research Letters, 27*(24), 3981–3984.

Galloway, D. L., & Hoffmann, J. (2007). The application of satellite differential SAR interferometry-derived ground displacements in hydrogeology. *Hydrogeology Journal, 15*(1), 133–154.

Hooper, A. (2010). A Statistical-cost approach to unwrapping the phase of InSAR time series. Proc. Fringe 2009 Workshop.

Hooper, A., Zebker, H., Segall, P., & Kampes, B. (2004). A new method for measuring deformation on volcanoes and other natural terrains using InSAR persistent scatterers. *Geophysical Research Letters, 31*, 611–615.

Hooper, A., Segall, P., & Zebker, A. (2007). Persistent scatterer interferometric synthetic aperture radar for crustal deformation analysis, with application to Volcan Alcedo, Galapagos. *Journal of Geophysical Research, 112*(B07407), 1–21.

Indirli, M., Nigro E., Kouris, L., Romanelli, F., & Zuccaro, G. (2010). Mitigation options for natural hazards, with a special focus on volcanic eruptions. Proceedings of the COST C26 Action Final Conference. Taylor & Francis group.

Kampes, B. M. (2005). Displacements Parameter Estimation using Permanent Scatterer Interferometry, DLR, Bibliotheks- und Informationswesen, Stuttgart.

Ketelaar, G. (2009). *Satellite radar interferometry subsidence monitoring techniques*. the Netherlands: Springer.

Lanari, R., Lundgren, P., Manzo, M., & Casu, F. (2004). Satellite radar interferometry time series analysis of surface deformation for Los Angeles, California. *Geophysical Research Letters, 31*, 1–5.

Peltzer, G., Rosen, P., Rogez, F., & Hudnut, K. (1998). Poro-elastic rebound along the Landers 1992 earthquake surface rupture. *Journal of Geophysical Research, 103*(B12), 30131–30145.

Peyret, M., Djamour, Y., Rizza, M., Ritz, J.-F., Hurtrez, J.-E., Goudarzi, M. A., Nankali, H., Chéry, J., Le Dortz, K., & Uri, F. (2008). Monitoring of the large slow Kahrod landslide in Alborz mountain range (Iran) by GPS and SAR interferometry. *Engineering Geology, 100*, 131–141.

Rott, H., Nagler, T., Rocca, F., Prati, C., Mazzotti, A., Keusen, H., Liener, S., & Tarchi, D. (2003). Geoinformation for European-wide integration: InSAR techniques and applications for monitoring landslides and subsidence (pp. 25–31). MillPress, Rotterdam

Singh, L. P., (2003). Application of SAR interferometry in landslide studies with special reference to generation of input data for statistical susceptibility assessment. MSc. degree thesis submitted to the international for geo-information science and earth observation.

Tesauro, M., Beradino, P., Lanari, R., Sansoti, E., Fornaro, G., & Franceschetti, G. (2000). Urban subsidence inside the City of Napoli (Italy) observed with synthetic aperture radar interferometry at Campi Flegrei caldera. *Journal of Geophysical Research, 27*, 1961–1964.